A General Switch-Mode Amplifier Design for Actuators Using MIMO Optimal Feedback Quantization

Jwu-Sheng Hu, *Member, IEEE*, and Keng-Yuan Chen, *Student Member, IEEE*

***Abstract*—This paper proposes a novel switch-mode power stage architecture for actuators. For a large number of actuators, the associated power amplifier becomes costly and bulky when each actuator is controlled by an independent amplifier. The proposed architecture allows actuators to share power amplifiers, thereby reducing the number of switching devices. This architecture is mapped into the graph theorem, and acceptable actuation states are analyzed. The switching method is controlled by multiple-input multiple-output optimal feedback quantization, which is designed to minimize a weighted measure of quantization distortion. Simulation and experimental results illustrate the effectiveness of the proposed scheme.**

***Index Terms*—Multiple-input multiple-output (MIMO) systems, optimal control, quantization, switching amplifier.**

I. Introduction

THE NEED to achieve control objectives using a large number of actuators has emerged in recent years. For example, a humanoid robot that mimics the human body requires a number of actuators [1], [2] to attain a vast degree of freedom. A large number of small mirrors moved by an array of actuators is needed to obtain the variable shape of a reflective surface [3], [4]. Virtual audio reality, which is a computer interface for visually impaired and blind users, uses an array of loudspeakers to manipulate the spatial sound [5]. Several topologies with reduced number of switches for motor driving are proposed in recent years [6]–[11], indicating that this study could potentially be useful in industrial applications. The easiest method of driving an actuator array is to use independent amplifiers for each actuator. However, for a large number of actuators, this one-to-one configuration can be inefficient and costly [12]. Consequently, several amplifier topologies have been developed. Notably, Cho *et al.* [13] investigated the power amplification architecture for dual actuators to reduce the number of switching elements needed. In [12], a matrix topology for amplifiers was developed for unidirectional actuators (i.e., current flows in one direction only). Thus, only $2N$ switching elements are necessary to drive $m = N^2$ actuators.

Another issue associated with sharing switching elements is the method of switching signal generation. Switch-mode amplifiers are commonly used in single actuators. The switching signal can be generated either by pulsewidth modulation (PWM) or sigma–delta methods. Several topologies subject to reducing the switching frequency [14], [15], switching loss [16] or torque/speed ripple [17], [18] are proposed. However, for the architecture of reduced switching elements, the switching signal for any amplifier cannot be independent because the number of actuators exceeds that of amplifiers. As a result, restricting the pattern of switching signals is necessary. A direct current-driving method was proposed in [13]; however, this method requires reference signals applied to the dual actuators to be complementary, thus limiting the scope of applications. A time-division PWM was proposed in [12], where only one actuator can be driven at one switching instant and the clock frequency requirement is high for a large number of actuators.

This paper investigates the possibility of reducing the number of switching elements in an actuation system containing a large number of actuators. The general case of this problem has not been discussed before. The proposed general actuation system allows actuators to share switching elements. In addition, the control of each actuator is bidirectional. The problem is formulated as a multiple-input multiple-output (MIMO) feedback quantization problem and is solved by extending the optimization technique proposed in [19]. The proposed method does not restrict the reference signal types as compared with that in [13]. Furthermore, by properly selecting filters in the optimization procedure, noise shaping can be performed to achieve improved tracking of reference signals in the desired bandwidth.

II. General Power Amplification System

A. Power Amplifier Scheme

Fig. 1(a) shows a full-bridge topology of a switching amplifier in a single actuator case. Each actuator terminal is connected to the junction (midpoint) of the half bridge, and the current direction through the actuator is controlled by turning the corresponding switching element on or off. For each half bridge, three switching states exist: Only the upper (lower) switch or none of the switches is turned on. The switching state is positive (negative) when the upper (lower) switch of the half bridge is turned on, i.e., the junction of the half bridge is connected to the positive supplied voltage (ground). The junction of the half bridge is a floating point when two switches are off. Three directions of the actuation current are obtained:

Manuscript received July 4, 2008; revised June 17, 2009. First published July 14, 2009; current version published November 6, 2009. This work was supported by the National Science Council of the Republic of China, Taiwan, under Contract NSC96-2218-E-009-018.

The authors are with the Department of Electrical and Control Engineering, National Chiao Tung University, Hsinchu 300, Taiwan (e-mail: jshu@cn.nctu.edu.tw; bettery.ece94g@nctu.edu.tw).

Digital Object Identifier 10.1109/TIE.2009.2027578

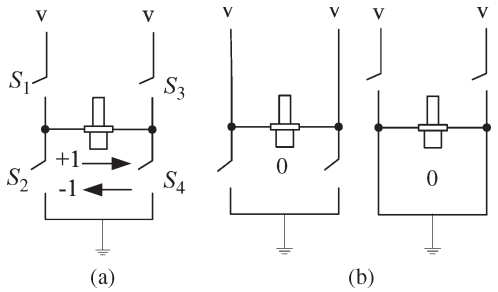

Fig. 1. (a) Traditional full-bridge power amplifier. (b) Switching methods of zero state.

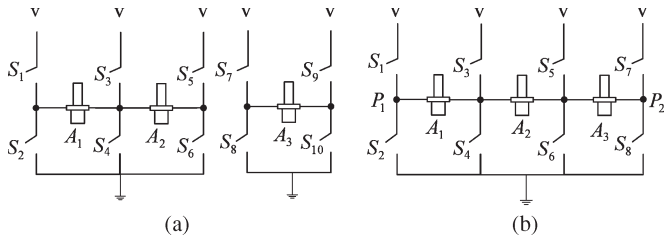

Fig. 2. Two kinds of actuation system for three actuators.

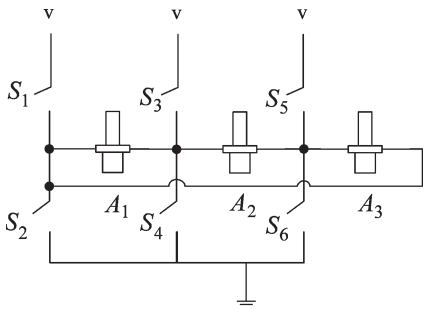

Fig. 3. Actuation system for three actuators.

$+1$, -1, and 0. Actuation state $+1$ is defined as current flowing through the actuator to the right, and in state -1, current flows to the left [Fig. 1(a)]. State 0 is defined as no current flowing from the supplied voltage side. This can be achieved by setting at least one of the half bridges in a floating state or both half bridges in the same state [Fig. 1(b)].

For two or more actuators, the topology of the switch-mode amplifier can be constructed from a broader perspective; thus, the number of switching elements can be reduced. Fig. 2 shows two cases with three actuators. The idea is to share a half bridge among actuators [e.g., pairs (S_3, S_4) in Fig. 2(a)]. The switches are further reduced to six when P_1 is connected to point P_2 [Fig. 2(b)] and pair (S_7, S_8) is replaced by (S_1, S_2), which results in a system in which each half bridge is shared by two actuators (Fig. 3). Therefore, given a number of actuators, several topologies exist, which result in different numbers of half bridges in a system. To explain topological variation, the actuation system is mapped to a simple graph defined by the graph theorem in [20], as shown in the subsequent section. A simple fact is that, if one actuator can be connected to any two half bridges, then with the number of half bridges n, the number of actuators that can be actuated is less than or equal to $C_2^n = n(n-1)/2$. Alternatively, the minimum number of half bridges needed to actuate $n(n-1)/2$ actuators is n. As a last note, we will not discuss the dead-time mechanism in the following context, although it is necessary in practice. It is to avoid complication in introducing the theory, and adding dead time can be another research topic following this general idea.

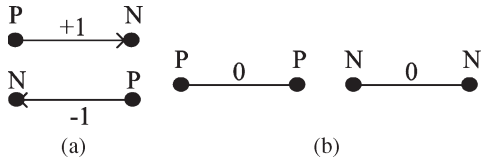

Fig. 4. Graphs that represent the actuation system in Fig. 1.

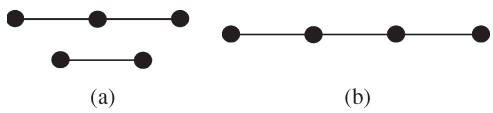

Fig. 5. Graphs that represent the actuation system in Fig. 2.

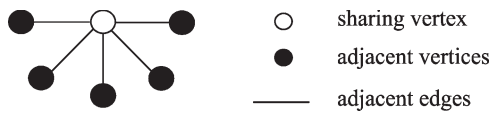

Fig. 6. Graph with definitions.

B. Definition Using Graph Theorem

The actuation system can be viewed as a *graph* [20]. The junction of a half bridge is the *vertex* in a graph, and the actuator connecting two vertices is an *edge*. Based on the mapping, the actuation systems can be represented by graphs (Figs. 4 and 5), where P (N) signifies that a half bridge is in positive (negative) state and the directed edge indicates the current status of an actuator. Vertex y is the *out-neighborhood* (*in-neighborhood*) of vertex x when the edge direction flows from x to y (from y to x). In addition, the "zero neighborhood" of vertex x indicates that no current exists between vertices y and x. Furthermore, the "adjacent edges" are defined as actuators sharing the same half bridge, and the vertex shared by adjacent edges is called a "sharing vertex." Moreover, the "adjacent vertices" are half bridges connected to the other side of adjacent edges (Fig. 6). Two properties are obtained based on the characteristics of the electric circuit.

Property 1: When a vertex has at least one out-neighborhood (in-neighborhood) and no in-neighborhood (out-neighborhood), the vertex is in positive (negative) state.

Property 2: The vertex is in floating state when it has at least one in-neighborhood and at least one out-neighborhood. Notably, supply voltage division occurs if and only if a floating vertex has at least one in-neighborhood and at least one out-neighborhood.

Property 1 is quite intuitive from the sense of an electrical circuit. The example of a dual-actuator system (Fig. 7) is utilized to explain Property 2. Assuming that vertex P_3 is an in-neighborhood and P_1 is an out-neighborhood of P_2, the switching method [Fig. 8(a)] results in system short circuit. Therefore, S_3 and S_4 must be turned off, and the dual actuators are in a serial connection [Fig. 8(b)]. Notice that the voltage drop across each actuator will be 1/2 of the supply voltage when

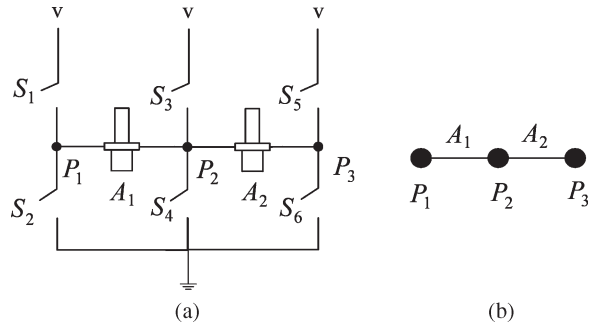

Fig. 7. (a) Actuation system for two actuators. (b) Corresponding graph.

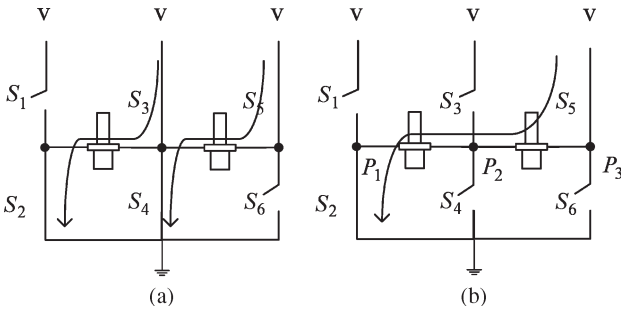

Fig. 8. Switching method of (a) $[-1\ -1]$ current state, which is not allowed, and (b) $[-1/2\ -1/2]$ state.

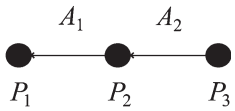

Fig. 9. Graph of the actuated system in Fig. 8(b).

both actuators are identical. Fig. 9 shows the corresponding graph in which vertex P_2 must be in the floating state. The same result can be obtained easily for other actuation systems and is omitted here. The analysis of switching states for a general connected actuation system is explained as follows.

C. Conditions of General Actuation System

Assume that the number of half bridges (actuators) in the general actuation system analyzed here is n (m), i.e., $m \leq n(n-1)/2$. Two conditions are imposed to obtain acceptable actuation states.

Condition 1: To protect switching elements from permanent damage, switching states that result in system short circuit are avoided.

Condition 2: To prevent adverse effects caused by mismatching actuators, states with supply voltage division between adjacent actuators are not considered.

Because each actuator has three actuation current types, 3^m actuation states may exist for a general actuation system. However, under Condition 1, shared switching elements cannot be turned on or off arbitrarily, i.e., the actuation current for actuators is not independent. An example in Fig. 10 shows that this state is not allowed. Therefore, the acceptable states for a general actuation system are less than 3^m, depending on the circuit architecture. The corresponding rules for Condition 1 are acquired by extending the rule proposed in [21].

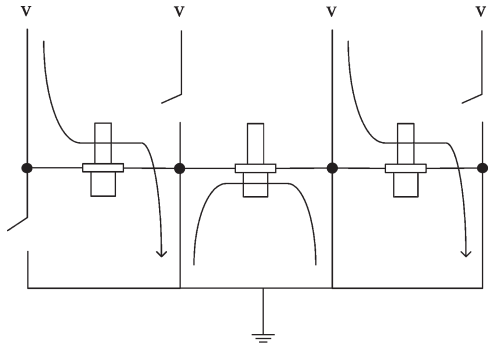

Fig. 10. Unacceptable switching method for a three-actuator system.

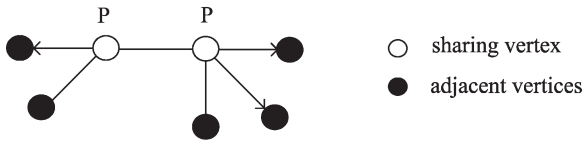

Fig. 11. Example for actuation rule one.

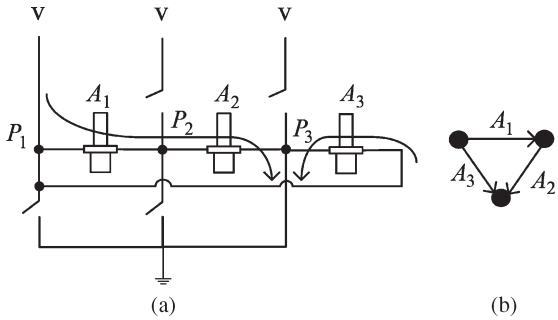

Fig. 12. (a) Current state for positive, floating, and negative states. (b) Corresponding graph.

Rule 1: Adjacent vertices of any two sharing vertices connected to the zero-state actuator must be either out-neighborhood (in-neighborhood) or zero neighborhood when sharing vertices are in positive (negative) state (Fig. 11).

Rule 2: If a path exists for which all current states of edges are zero, all adjacent vertices of vertices on the path must be in-neighborhood (out-neighborhood) or zero neighborhood when one sharing vertex on the path is in negative (positive) state.

Using these rules, one can obtain the acceptable current actuation states for a specific topology.

From the half-bridge perspective, the problem of finding the number of acceptable actuation states is simple. As each half bridge also has three switching methods, 3^n switching states exist for n half bridges. Notably, none of the 3^n switching states results in system short circuit. Each state corresponds to the current status of actuators. For example, the switching state [positive, floating, and negative] of the system Fig. 3 yields actuation current as shown in Fig. 12. From a power delivery perspective, some switching states correspond to the same current status. For instance, zero current status for all actuators is achieved by setting all half bridges in positive state or by setting one half bridge floating and others positive.

Condition 2 requires that supply voltage division among actuators must be avoided. Based on Property 2, voltage division occurs when a floating vertex has both in- and

out-neighborhoods. Therefore, this paper proposes a rule for a floating vertex.

Rule 3: The adjacent edges of a floating vertex must all be zero neighborhoods, suggesting that, if one adjacent vertex is in positive (negative) state, other adjacent vertices must be either in positive (negative) or in floating state. Furthermore, if a path exists on which all vertices are floating, then all adjacent vertices on the path must be zero neighborhood.

Proposition 1 depicts the conditions of a connected actuation system.

Proposition 1: All current actuation states satisfying Conditions 1 and 2 can be achieved using only positive and negative switching states instead of three states (positive, negative, and floating).

Proof: First, consider a case with a single floating vertex. Because the sharing voltage is prohibited, the zero-state actuator occurs when a vertex is in the floating state. Assume that the floating vertex has p adjacent edges; these p adjacent edges must be in zero state, which can be achieved by the following two methods: All these p adjacent vertices are set in positive or negative state. The same state (all adjacent edges are in zero state) is obtained when the sharing vertex is set to the same state as the adjacent vertices instead of floating. Moreover, the same conclusion is obtained when one considers the path on which all vertices are in floating states. ■

Therefore, under Conditions 1 and 2, 2^n switching methods exist in a general actuation system. In the power delivery viewpoint, the actuating currents of all half bridges in positive state are the same as all of them are in negative state. Hence, these 2^n switching methods correspond to $2^n - 1$ actuation currents, which are exactly the acceptable actuation states of the proposed general actuation system.

To represent the current states in the vector form, vertices are labeled from $1 \sim n$. The current flowing through the actuator is defined as $+1$ when the direction flows from a small number of vertices to a large number ones, i.e., the current state of the system in Fig. 9 is $[-1/2 \quad -1/2]^{\mathrm{T}}$ and that for Fig. 12 is $[+1/2 \quad +1/2 \quad +1]^{\mathrm{T}}$.

In the next section, the MIMO optimal decision algorithm is proposed to control the general actuation system for tracking a prescribed band-limited reference signal.

III. Switching Command Generation via Optimal Feedback Quantization

Given the number of actuators and the proposed power stage topology, as shown in the preceding section, the next question is how to generate the control command for each switching element to achieve actuator control objectives. For a single actuator, Hu *et al.* [22]–[24] proposed a generalized sigma–delta modulation method to generate switching commands at a high sampling rate. This study extends this single-input single-output (SISO) modulator to the MIMO setting by formulating the problem as a constrained optimization problem.

A. Problem Formulation

Assume that the number of actuators (half bridges) in the system is m (n). Given input signals $\mathbf{r} \in R^m$ and an m-input

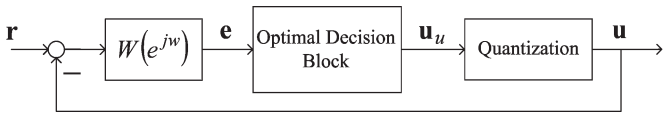

Fig. 13. Block diagram of optimal MIMO feedback quantization.

m-output filter matrix W, the problem of reference signal tracking is a constrained optimization problem: Find the optimal control signals $\mathbf{u}$ from a finite set of prescribed vectors S, such that the cost function V is minimized. The cost function is defined as the sum of the m instantaneously filtered error power

$$V \triangleq \mathbf{e}^{\mathrm{T}} P \mathbf{e}, \qquad \mathbf{e} \in R^m; \quad P^{\mathrm{T}} = P \in R^{m \times m} \tag{1}$$

where $P \geq 0$, and $\mathbf{e}$ is the sample of filtered error $E(e^{jw})$ defined as

$$E(e^{jw}) = W(e^{jw}) \left(R(e^{jw}) - U(e^{jw}) \right) \tag{2}$$

where the elements of vectors $R(e^{jw})$ and $U(e^{jw})$ are discrete-time Fourier transforms of elements $\mathbf{r}$ and $\mathbf{u}$, respectively, and $W(e^{jw})$ is the frequency response of the filter matrix W. Filter matrix W can be written as

$$W = \begin{bmatrix} w_{11} & w_{12} & \cdots & w_{1m} \\ w_{21} & w_{22} & & \\ \vdots & & \ddots & \\ w_{m1} & & & w_{mm} \end{bmatrix}$$

where w_{ij} is the SISO transfer function from the jth input to the ith output. Thus, the modulator quantizes signals $\mathbf{r}$ such that the power of the difference between $\mathbf{r}$ and $\mathbf{u}$ is minimized in the frequency band that the magnitude response of w_{ij} is large. Assume that the order of SISO transfer functions w_{ij} are all p; W can then be expressed in the state-space form

$$\begin{aligned} x(k+1) &= Ax(k) + B\left(\mathbf{r}(k) - \mathbf{u}(k)\right) \\ \mathbf{e}(k) &= Cx(k) + D\left(\mathbf{r}(k) - \mathbf{u}(k)\right) \end{aligned} \tag{3}$$

where $x \in R^{mp}$, $\mathbf{u} \in R^m$, $A \in R^{mp \times mp}$, $B \in R^{mp \times m}$, $C \in R^{m \times mp}$, and $D \in R^{m \times m}$. Notably, vectors in constrained set S are the acceptable actuation current states of the general actuation system described in Section II-C.

B. Optimal MIMO Feedback Quantization

Fig. 13 shows the block diagram of the optimal MIMO feedback quantization. The optimal decision algorithm computes the optimal control command $\mathbf{u}_u$, given the error signals. $\mathbf{u}_u$ is derived by minimizing V. First, substituting (3) into (1) yields

$$\begin{aligned} V &= \mathbf{e}(k)^{\mathrm{T}} P \mathbf{e}(k) \\ &= \left(Cx(k) + D(\mathbf{r}(k) - \mathbf{u}(k))\right)^{\mathrm{T}} P \left(Cx(k) + D\left(\mathbf{r}(k) - \mathbf{u}(k)\right)\right) \\ &= f\left(x(k), \mathbf{r}(k)\right) + \mathbf{u}(k)^{\mathrm{T}} D^{\mathrm{T}} P D \mathbf{u}(k) \\ &\quad - 2\left(Cx(k) + D\mathbf{r}(k)\right)^{\mathrm{T}} P D \mathbf{u}(k) \end{aligned} \tag{4}$$

where $f(x(k), \mathbf{r}(k))$ is a term independent of $\mathbf{u}$. The optimal solution to (4) is obtained by solving $(\partial V / \partial \mathbf{u}) = 0$

$$u_u = D^{-1}\left(Cx(k) + D\mathrm{r}(k)\right). \tag{5}$$

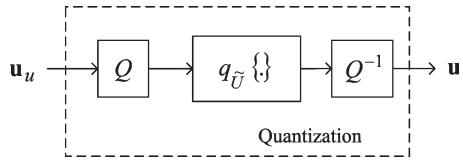

Fig. 14. Diagram of quantization block.

The optimal control command is then quantized according to the limitation due to power stage topology, as described in Section II. The quantization block in Fig. 13 is an m-dimensional quantizer, which is defined as (Fig. 14)

$$\mathbf{u} = Q^{-1} q_{\widetilde{U}}\{Q\mathbf{u}_u\} \tag{6}$$

where $Q^{\mathrm{T}}Q = D^{\mathrm{T}}PD$, and $q_{\widetilde{U}}\{.\}$ is the nearest neighbor vector quantizer defined in Definition I [19].

Definition 1 (Nearest Neighbor Vector Quantizer): For a set of vectors $\widetilde{U} = \{\widetilde{\nu}_1, \widetilde{\nu}_2, \ldots, \widetilde{\nu}_{(K_r)}\} \subset R^m$, the nearest neighbor quantizer is defined as a mapping $q_{\widetilde{U}} : R^m \to \widetilde{U}$, which assigns to each vector $c \in R^m$ the closest element of $\widetilde{U}$ (as measured by the Euclidean norm), i.e., $q_{\widetilde{U}}(c) = \widetilde{\nu}_i \in \widetilde{U}$ if and only if c satisfies $\|c - \widetilde{\nu}_i\| \le \|c - \widetilde{\nu}_j\| \quad \forall\, \widetilde{\nu}_i \ne \widetilde{\nu}_j, \widetilde{\nu}_j \in \widetilde{U}$. ■

To demonstrate that the switching state $\mathbf{u}$ in (6) results in the smallest V, $\mathbf{u} = Q^{-1}\widetilde{\nu}$ is first substituted into (4)

$$V = f(x(k), \mathbf{r}(k)) + \widetilde{\nu}(k)^{\mathrm{T}}\widetilde{\nu}(k) - 2\big(Cx(k) + D\mathbf{r}(k)\big)^{\mathrm{T}} D^{-\mathrm{T}} Q^{\mathrm{T}} \widetilde{\nu}(k) \tag{7}$$

where $f(x(k), \mathbf{r}(k))$ is independent of $\mathbf{u}$. Thus, the level sets of V in (7) are spheres centered at $QD^{-1}(Cx(k) + D\mathbf{r}(k)) = Q\mathbf{u}_u$.

As a result, V is minimized when $\widetilde{\nu} = q_{\widetilde{U}}\{Q\mathbf{u}_u\}$ or, alternatively, when $\mathbf{u} = Q^{-1}\widetilde{\nu} = Q^{-1}q_{\widetilde{U}}\{Q\mathbf{u}_u\}$. Hence, the image of the nearest neighbor vector quantizer $q_{\widetilde{U}}\{.\}$ is

$$\tilde{U} = \{\tilde{\nu}_1, \tilde{\nu}_2, \ldots, \tilde{\nu}_{K_r}\} \subset R^m \qquad \text{with } \tilde{\nu}_i = Q\nu_i,\ \nu_i \in S$$

where S is the set of acceptable current states for the general actuation system, and K_r is the number of acceptable states $2^n - 1$.

The system performance is analyzed to determine the efficiency of the proposed optimal quantization control method.

C. Performance Analysis and Quantization Error

For a SISO system, the optimal quantization algorithm is the generalized sigma–delta modulator [19]. The conventional analytical method for the sigma–delta modulator obtains the output noise spectrum from the noise transfer function of the linear model, which treats the error signal induced by the quantizer as a white noise [25]. An alternative interpretation of the noise-shaping mechanism in the sigma–delta modulator, which treats quantizer input as a modulation error, was recently presented in [26] and [27] to reflect the effect of the sampling frequency.

Here, quantization error is defined as the difference between the input and output of the nearest neighbor vector quantizer, which is the same as the conventional method. The concept of error analysis is extended from [23] to the MIMO system. By using MIMO optimal feedback quantization, the error signal $\mathbf{e}$ is strongly related to quantization error. The $\mathbf{e}$ in (3) is written as follows using (5) and (6):

$$\begin{aligned}\mathbf{e}(k) &= Cx(k) + D\left(\mathbf{r}(k) - \mathbf{u}(k)\right) \\ &= Cx(k) + D\mathbf{r}(k) - DQ^{-1}q_{\tilde{U}}\left\{Q\mathbf{u}_u(k)\right\} \\ &= DQ^{-1}\left(Q\mathbf{u}_u(k) - q_{\tilde{U}}\left\{Q\mathbf{u}_u(k)\right\}\right).\end{aligned} \tag{8}$$

Therefore, the minimization of $\mathbf{e}$ reflects the difference between the input and output of the nearest neighbor vector quantizer ($Q\mathbf{u}_u$ and $q_{\widetilde{U}}\{Q\mathbf{u}_u\}$). Furthermore, if matrix P [see (1) and (6)] is selected as an identity matrix, filtered error $\mathbf{e}$ then becomes

$$\begin{aligned}\mathbf{e}(k) &= DD^{-1}\left(Q\mathbf{u}_u(k) - q_{\tilde{U}}\left\{Q\mathbf{u}_u(k)\right\}\right) \\ &= Q\mathbf{u}_u(k) - q_{\tilde{U}}\left\{Q\mathbf{u}_u(k)\right\}\end{aligned}$$

which is the exact quantization error. To elucidate the effect of noise shaping, the Fourier transform of output $\mathbf{u}$ is expressed as follows from (2):

$$U(e^{jw}) = R(e^{jw}) - W^{-1}(e^{jw})E(e^{jw}). \tag{9}$$

If the inverse of the transfer matrix W^{-1} is denoted as

$$W^{-1} = \begin{bmatrix} h_{11} & h_{12} & \cdots & h_{1m} \\ h_{21} & h_{22} & & \\ \vdots & & \ddots & \\ h_{m1} & & & h_{mm} \end{bmatrix}$$

$$R(e^{jw}) = \begin{bmatrix} R_1(e^{jw}) \\ R_2(e^{jw}) \\ \vdots \\ R_m(e^{jw}) \end{bmatrix} \qquad U(e^{jw}) = \begin{bmatrix} U_1(e^{jw}) \\ U_2(e^{jw}) \\ \vdots \\ U_m(e^{jw}) \end{bmatrix}$$

$$E(e^{jw}) = \begin{bmatrix} E_1(e^{jw}) \\ E_2(e^{jw}) \\ \vdots \\ E_m(e^{jw}) \end{bmatrix}$$

then the ith actuation output $U_i(e^{jw})$ is written as

$$U_i(e^{jw}) = R_i(e^{jw}) - \sum_{l=1}^{m} h_{il}E_l(e^{jw}). \tag{10}$$

As a result, each output actuation command contains two parts of the signals: The first term is the corresponding input signal R_i, and the second term is the sum of quantization errors, which is the residual error E_l from each channel, filtered by the inverse of the system filters h_{il}. Consequently, W^{-1} is responsible for spectrally shaping the noise in the MIMO system. When the bandwidth of reference signals is w_B, $w_B \in (0, \pi)$ and π correspond to the half sampling frequency;

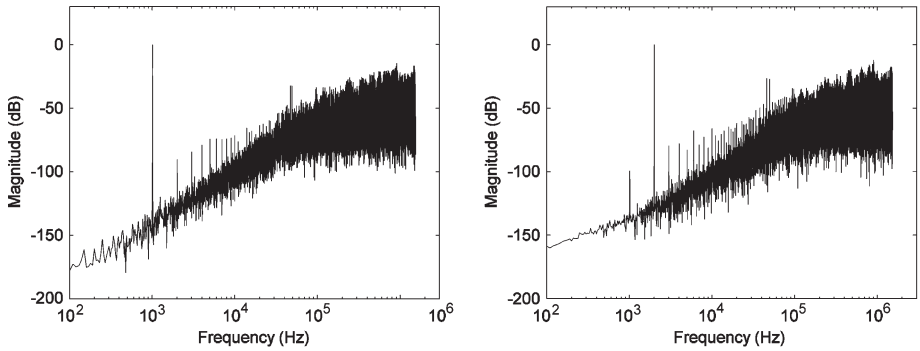

Fig. 15. Simulation results: DFT of outputs. (a) Output one. (b) Output two.

the signal-to-noise ratio (SNR) of the ith channel is represented as [26]

$$\text{SNR}_i = \int_0^{w_B} \left| \frac{R_i(e^{jw})}{\sum_{l=1}^{m} h_{il} E_i(e^{jw})} \right|^2 dw. \tag{11}$$

If all reference signals are independent, one can design the shaping filter matrix W in a diagonal form, i.e.,

$$W = \begin{bmatrix} w_{11} & 0 & \cdots & 0 \\ 0 & w_{22} & & \vdots \\ \vdots & & \ddots & 0 \\ 0 & \cdots & 0 & w_{mm} \end{bmatrix}$$

$$W^{-1} = \begin{bmatrix} w_{11}^{-1} & 0 & \cdots & 0 \\ 0 & w_{22}^{-1} & & \vdots \\ \vdots & & \ddots & 0 \\ 0 & \cdots & 0 & w_{mm}^{-1} \end{bmatrix}.$$

The SNR then becomes

$$\text{SNR}_i = \int_0^{w_B} \left| \frac{R_i(e^{jw})}{w_{ii}^{-1} E_i(e^{jw})} \right|^2 dw \tag{12}$$

indicating that the SNR of the ith channel depends only on the ith quantization error. However, cross-talk effect between channels may exist due to switching limitations of general actuation systems. This affects the magnitude of $\mathbf{e}$. Therefore, for the same shaping filter matrix W, the SNR of each channel may differ for different configurations, and this effect is reflected in the filtered error $\mathbf{e}$.

IV. Examples and Simulation Results

Two examples are shown to verify the effectiveness of MIMO optimal control for tracking reference signals and the possibility of reducing the number of switching elements in the actuation system. In the first example, the proposed architecture is applied to a dual-channel class-D audio amplifier. Both simulation and experimental results are shown in this example. The second example adopts three actuation architectures for a four-actuator system (Fig. 20). Simulation results are provided to verify the proposed topology. Without loss of generality, all the signals are normalized to one in this section.

A. Example 1: Dual-Channel Class-D Audio Amplifier

Conventional class-D amplification typically uses half-bridge or full-bridge power amplifiers. Here, an actuation system for two speakers (Fig. 7) is used. Compared with the half bridge, the system in this study avoids the circuit to generate mid-voltage. Moreover, the switching elements needed are reduced from eight to six as compared to independent full-bridge amplifier for each speaker. A weighting filter matrix $W(z)$ is selected as a diagonal form because reference signals are independent

$$W(z) = \begin{bmatrix} w_{11}(z) & w_{12}(z) \\ w_{21}(z) & w_{22}(z) \end{bmatrix} = \begin{bmatrix} w(z) & 0 \\ 0 & w(z) \end{bmatrix}.$$

Since the input audio signal bandwidth is 22.05 kHz, the performance is characterized at low frequency. Therefore, $w(z)$ is selected as a second-order low-pass filter with a cutoff frequency 150 kHz. The system state-space matrices are

$$A = \begin{bmatrix} 0 & -1 & 0 & 0 \\ 1 & 2 & 0 & 0 \\ 0 & 0 & 0 & -1 \\ 0 & 0 & 1 & 2 \end{bmatrix} \qquad B = \begin{bmatrix} -0.44 & 0 \\ 0.53 & 0 \\ 0 & -0.44 \\ 0 & 0.53 \end{bmatrix}$$

$$C = \begin{bmatrix} 0 & 1 & 0 & 0 \\ 0 & 0 & 0 & 1 \end{bmatrix} \qquad D = \begin{bmatrix} 1.24 & 0 \\ 0 & 1.24 \end{bmatrix}.$$

The number of acceptable current states is $2^3 - 1 = 7$, and

$$S = \left\{ \begin{bmatrix} -1 \\ 0 \end{bmatrix}, \begin{bmatrix} -1 \\ 1 \end{bmatrix}, \begin{bmatrix} 0 \\ -1 \end{bmatrix}, \begin{bmatrix} 0 \\ 0 \end{bmatrix}, \begin{bmatrix} 0 \\ 1 \end{bmatrix}, \begin{bmatrix} 1 \\ 0 \end{bmatrix}, \begin{bmatrix} 1 \\ -1 \end{bmatrix} \right\}$$

where the elements of vectors in S are the current states of two loudspeakers, respectively.

Two sinusoidal waves, one at 1 kHz and the other at 2 kHz with amplitude 0.3 sampled at 48 kHz, are applied to the system as reference signals. The spectrums of the output signals applied to loudspeakers are obtained by taking the discrete Fourier transform of the elements of $\mathbf{u}(k)$. The frequency domain analysis of simulation results is shown in Fig. 15. The resulting signal-to-noise plus distortion ratios (SNDRs) within

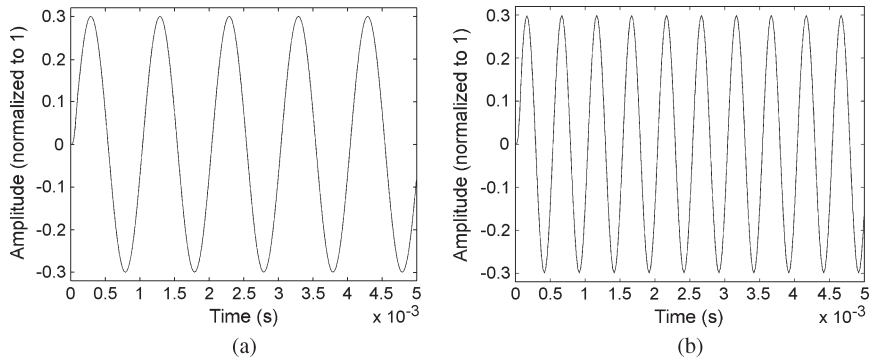

Fig. 16. Simulation results: Waveform of outputs after filtering. (a) Output one (1 kHz). (b) Output two (2 kHz).

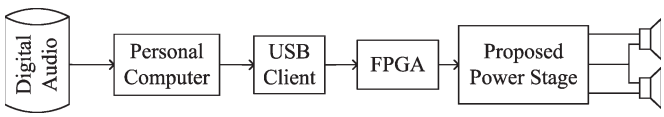

Fig. 17. Block diagram of experimental platform.

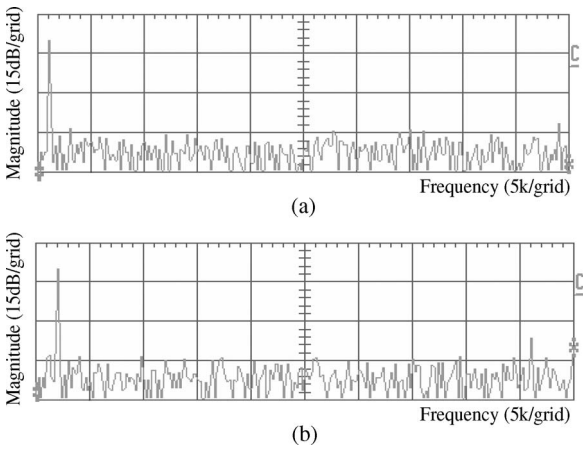

Fig. 18. Experimental results: DFT of outputs. (a) Output one. (b) Output two.

the bandwidth [0, 22.05 kHz] are 97 and 98 dB. The SNDR already characterizes the cross talk by viewing its negative values (e.g., -97 and -98 dB). Fig. 16 shows the resulting output current filtered by a low-pass filter cutoff at 22.05 kHz.

To realize the proposed system, an experimental platform is designed, as shown in Fig. 17. The Universal Serial Bus client receives dual-channel 48-kHz digital audio streams from a personal computer. The audio data are then up-sampled to 3.072 MHz and fed into the optimal feedback quantization system. The up sampling and the modulator are implemented by a field-programmable gate array. The general actuation system in this example is composed of three n-MOS and three p-MOS. The frequency/time domain analyses of the implemented system are shown in Figs. 18 and 19. It is shown in Fig. 18 that no cross talk exists in channels, and Fig. 19 shows a good signal tracking performance.

B. Example 2: Actuation Systems for Four Actuators

Suppose that a system has four identical and four independent reference signals that have to be tracked. The weighting filter $W(z)$ can be written as

$$W(z) = \begin{bmatrix} w_{11}(z) & w_{12}(z) & w_{13}(z) & w_{14}(z) \\ w_{21}(z) & w_{22}(z) & w_{23}(z) & w_{24}(z) \\ w_{31}(z) & w_{32}(z) & w_{33}(z) & w_{34}(z) \\ w_{41}(z) & w_{42}(z) & w_{43}(z) & w_{44}(z) \end{bmatrix} = \begin{bmatrix} w(z) & 0 & 0 & 0 \\ 0 & w(z) & 0 & 0 \\ 0 & 0 & w(z) & 0 \\ 0 & 0 & 0 & w(z) \end{bmatrix}. \tag{13}$$

The operating frequency is set at 3.072 MHz when the bandwidth of inputs is within 24 kHz, thereby yielding an oversampling ratio of 64. Furthermore, filter $w(z)$ is selected as a second-order filter with a large magnitude response in the 0–24-kHz frequency band, i.e., $w(z)$ is designed as a low-pass filter with a cutoff frequency of 130 kHz. The transfer function of $w(z)$ is

$$w(z) = \frac{1.207z^2 - 1.964z + 0.8288}{z^2 - 2z + 1}. \tag{14}$$

The quantization block (Figs. 13 and 14) computes the optimal output $\mathbf{u}$ such that the cost function $V = \mathbf{e}^{\mathrm{T}}\mathbf{e}$ is minimized. The fully independent control of each actuator requires four H-bridges that contain 16 switching elements. The half bridges in Fig. 20 are labeled as P_i, where $i = 1, 2, 3, 4,$ and 5, and actuators are A_j, where $j = 1, 2, 3,$ and 4. Therefore, the requirements of switching elements in the configurations in Fig. 20(a)–(c) are ten, ten, and eight, respectively. By definition, the acceptable current set S is obtained. For example, the set S for the system in Fig. 20(c) is

$$S = \left\{ \begin{bmatrix} 0 \\ 0 \\ 0 \\ 0 \end{bmatrix}, \begin{bmatrix} 0 \\ 0 \\ 1 \\ 0 \end{bmatrix}, \begin{bmatrix} 0 \\ 1 \\ 0 \\ 1 \end{bmatrix}, \begin{bmatrix} 0 \\ 1 \\ 1 \\ 1 \end{bmatrix}, \begin{bmatrix} 1 \\ 0 \\ 0 \\ -1 \end{bmatrix}, \begin{bmatrix} 1 \\ 0 \\ 1 \\ -1 \end{bmatrix}, \begin{bmatrix} 1 \\ 1 \\ 0 \\ 0 \end{bmatrix}, \begin{bmatrix} 1 \\ 1 \\ 1 \\ 0 \end{bmatrix}, \begin{bmatrix} -1 \\ -1 \\ -1 \\ 0 \end{bmatrix}, \begin{bmatrix} -1 \\ -1 \\ 0 \\ 0 \end{bmatrix}, \begin{bmatrix} -1 \\ 0 \\ -1 \\ 1 \end{bmatrix}, \begin{bmatrix} -1 \\ 0 \\ 0 \\ 1 \end{bmatrix}, \begin{bmatrix} 0 \\ -1 \\ -1 \\ -1 \end{bmatrix}, \begin{bmatrix} 0 \\ -1 \\ 0 \\ -1 \end{bmatrix}, \begin{bmatrix} 0 \\ 0 \\ -1 \\ 0 \end{bmatrix} \right\}$$

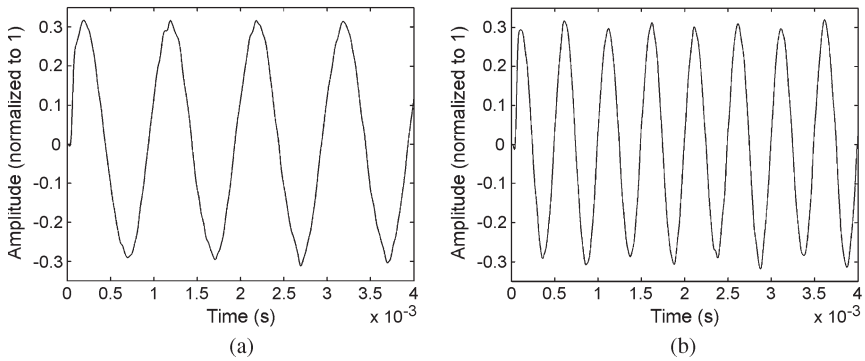

Fig. 19. Experimental results: Waveform of outputs after filtering. (a) Output one (1 kHz). (b) Output two (2 kHz).

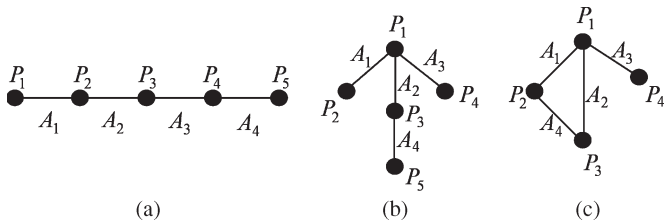

Fig. 20. Three kinds of the actuation architectures for a four-actuator system.

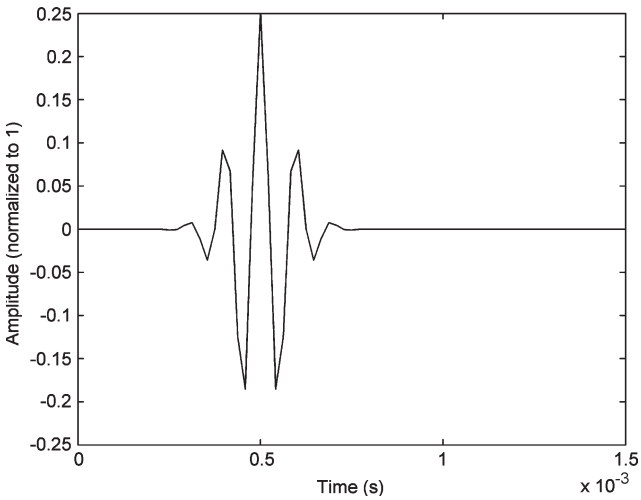

Fig. 21. Nonperiodic reference signal.

where the jth element of vectors in S is the current state of actuator A_j.

Two periodic reference signals, which are sinusoid and trapezoid, and a nonperiodic signal (see Fig. 21), all sampled at 48 kHz, are applied to the systems. The frequency of sinewaves is 1 kHz and that of trapezoid is 100 Hz with 2.5-ms rising (falling) time. The frequency analyses of outputs that correspond to the sinusoidal reference signal are derived to calculate SNR of the proposed topology, and the time responses of output voltages for all inputs are used to confirm the signal tracking performance. The mean powers of the tracking errors within the reference bandwidth are used, and they are denoted as T_{r1}, T_{r2}, and T_{r3} for the sinusoid, trapezoid, and nonperiodic inputs, respectively.

Table I shows the simulation results. The case of using a full bridge for each actuator is denoted as "single." Performance degradation in SNRs for all the topologies in Fig. 20 can

TABLE I
PERFORMANCE OF OUTPUT SIGNAL $\mathbf{u}(k)$ APPLIED TO ACTUATORS IN FIG. 20

Actuator	SNR(dB)	THD(%)	T_{r1}	T_{r2}	T_{r3}
Single	92.80	0.102	0.179	0.190	0.134
A_1(a)	87.54	0.147	0.243	0.365	0.237
A_2(a)	88.60	0.139	0.233	0.375	0.229
A_3(a)	86.40	0.157	0.231	0.370	0.225
A_4(a)	87.54	0.147	0.242	0.374	0.234
A_1(b)	89.25	0.144	0.178	0.188	0.134
A_2(b)	88.07	0.152	0.190	0.196	0.141
A_3(b)	89.25	0.144	0.178	0.188	0.134
A_4(b)	89.48	0.137	0.190	0.200	0.141
A_1(c)	85.53	0.231	--	--	--
A_2(c)	80.61	0.221	--	--	--
A_3(c)	92.25	0.081	0.178	0.188	0.136
A_4(c)	79.83	0.243	--	--	--

be observed. The topology in Fig. 20(c) results in the lowest SNR, and the variation of performances is large, indicating that performances degrade when the number of switching elements is too small (eight switching elements as compared with 16 in four H-bridges).

In addition, for the same number of switching elements, the topology in Fig. 20(b) exhibits a better and uniform SNR across all actuators compared with the one in Fig. 20(a). The same result is obtained, considering the tracking performances. In particular, for the trapezoid reference signals, the error power in Fig. 20(a) is almost twice as high as that in Fig. 20(b). For the case in Fig. 20(c), the tracking errors of actuators A_1, A_2, and A_4, which share three half bridges to each other, are all larger than the normalized amplitude of the reference signal. The reason is that there is only two degrees of freedom in the circular connection of those three actuators. As a result, poor performance occurs when three independent references are applied to those three actuators. Notably, the tracking performance still maintains for A_3, which only shares one half bridge with other two actuators. These observations are interesting and warrant further study for all possible configurations.

V. CONCLUSION

The switch-mode amplifier for driving multiple actuators has been viewed in a broad perspective in this paper. To reduce the number of switches, actuators share half bridges. The proposed

architecture and electrical characteristics can be mapped to a digraph in the graph theorem. The number of acceptable actuation states for the system is analyzed. The MIMO optimal feedback quantization algorithm is used to produce switching commands based on the constrained set of acceptable actuation states. The algorithm produces decisions for turning each switching element on or off to minimize the power of quantization error in tracking of reference signals. Two examples have been provided in this paper, and simulation results have confirmed the effectiveness of the proposed scheme. This work opens a new direction for designing the power stage for multiple actuators (or actuator arrays) and has potential applications, such as microelectromechanical system, which require distributed actuators. Further research topics, such as dead-time control for switches, stability, shaping filter matrix design, relationship between topology and performance, quantizer efficiency, and possible utilization of graph theory, remain to be explored.

ACKNOWLEDGMENT

The authors would like to thank the reviewers for their valuable comments.

REFERENCES

[1] L. Flemming and S. Mascaro, "Control of scalable wet SMA actuator arrays," in *Proc. Robot. Autom. Conf.*, Barcelona, Spain, 2005, pp. 1338–1343.
[2] K. J. Cho and H. Asada, "Multi-axis SMA actuator array for driving anthropomorphic robot hand," in *Proc. Robot. Autom. Conf.*, Barcelona, Spain, 2005, pp. 1356–1361.
[3] G. B. Thomas, R. K. Mali, J. K. Dorton, J. Perreault, N. Vandelli, M. N. Horenstein, and D. A. Castanon, "Continuous-membrane surface-micromachined silicon deformable mirror," *Opt. Eng.*, vol. 36, no. 5, pp. 1354–1360, May 1997.
[4] G. Stein and D. Gorinevsky, "Design of surface shape control for large two-dimensional arrays," *IEEE Trans. Control Syst. Technol.*, vol. 13, no. 3, pp. 422–433, May 2005.
[5] C. Frauenberger and M. Noisternig, "3D audio interfaces for the blind," in *Proc. Int. Conf. Auditory Display*, Boston, MA, 2003, pp. 280–283.
[6] C. B. Jacobian, T. M. Oliveira, and E. R. C. da Silva, "Control of the single-phase three-leg AC/AC converter," *IEEE Trans. Ind. Electron.*, vol. 53, no. 2, pp. 467–476, Apr. 2006.
[7] C. B. Jacobian, E. C. dos Santos, Jr., M. B. R. Correa, and E. R. C. da Silva, "AC motor drives with a reduced number of switches and boost inductors," *IEEE Trans. Ind. Appl.*, vol. 43, no. 1, pp. 30–39, Jan./Feb. 2007.
[8] P. Lezana, J. Rodriguez, and D. A. Oyarzun, "Cascaded multilevel inverter with regeneration capability and reduced number of switches," *IEEE Trans. Ind. Electron.*, vol. 55, no. 3, pp. 1059–1066, Mar. 2008.
[9] M. Chomat and T. A. Lipo, "Adjustable-speed single-phase IM drive with reduced number of switches," *IEEE Trans. Ind. Appl.*, vol. 39, no. 3, pp. 819–825, May/Jun. 2003.
[10] E. Ledezma, B. McGrath, A. Munoz, and T. A. Lipo, "Dual AC-drive system with a reduced switch count," *IEEE Trans. Ind. Appl.*, vol. 37, no. 5, pp. 1325–1333, Sep./Oct. 2001.
[11] C. B. Jacobian, I. S. Freitas, C. R. da Silva, M. B. R. Correa, and E. R. C. da Silva, "Reduced switch-count six-phase AC motor drive systems without input reactor," *IEEE Trans. Ind. Electron.*, vol. 55, no. 5, pp. 2024–2032, May 2008.
[12] K. J. Cho, S. Au, and H. H. Asada, "Large-scale servo control using a matrix wire network for driving a large number of actuators," in *Proc. Robot. Autom. Conf.*, Taipei, Taiwan, 2003, pp. 646–651.
[13] K. M. Cho, W. S. Oh, W. S. Chung, and H. J. Kim, "A new class-D stereo audio amplifier using direct speaker current control," in *Proc. 35th Annu. IEEE Power Electron. Spec. Conf.*, Aachen, Germany, 2004, pp. 1308–1310.
[14] P. Zanchetta, D. B. Gerry, V. G. Monopoli, J. C. Clare, and P. W. Wheeler, "Predictive current control for multilevel active rectifiers with reduced switching frequency," *IEEE Trans. Ind. Electron.*, vol. 55, no. 1, pp. 163–172, Jan. 2008.
[15] A. Sikorski and T. Citko, "Current controller reduced switching frequency for VS-PWM inverter used with AC motor drive applications," *IEEE Trans. Ind. Electron.*, vol. 45, no. 5, pp. 792–801, Oct. 1998.
[16] D. D. C. Lu, D. K. W. Cheng, and Y. S. Lee, "A single-switch continuous-conduction-mode boost converter with reduced reverse-recovery and switching losses," *IEEE Trans. Ind. Electron.*, vol. 50, no. 4, pp. 767–776, Aug. 2003.
[17] N. R. N. Idris and A. H. M. Yatim, "Direct torque control of induction machines with constant switching frequency and reduced torque ripple," *IEEE Trans. Ind. Electron.*, vol. 51, no. 4, pp. 758–767, Aug. 2004.
[18] Y. S. Lai, W. K. Wang, and Y. C. Chen, "Novel switching techniques for reducing the speed ripple of AC drives with direct torque control," *IEEE Trans. Ind. Electron.*, vol. 51, no. 4, pp. 768–775, Aug. 2004.
[19] D. E. Quevedo and G. C. Goodwin, "Multi-step optimal analog-to-digital conversion," *IEEE Trans. Circuits Syst. I, Reg. Papers*, vol. 52, no. 3, pp. 503–515, Mar. 2005.
[20] G. Chartrand and O. R. Oellermann, "An introduction to graphs," in *Applied and Algorithmic Graph Theory*. New York: McGraw-Hill, 1993.
[21] J. S. Hu and K. Y. Chen, "A novel switch mode amplifier design for actuator array using MIMO optimal feedback quantization," in *Proc. Amer. Control Conf.*, New York, 2007, pp. 2612–2617.
[22] J. S. Hu and K. Y. Chen, "Implementation of a full digital amplifier using feedback quantization," in *Proc. Amer. Control Conf.*, Minneapolis, MN, 2006, pp. 2759–2764.
[23] J. S. Hu and K. Y. Chen, "An FPGA implementation of finite horizon constrained optimization for a full digital amplifier," in *Proc. Amer. Control Conf.*, New York, 2007, pp. 4047–4052.
[24] J. Hu and S.-H. Yu, "Analysis and design of 1-bit noise-shaping quantizer using variable structure control approach," *Asian J. Control*, vol. 7, no. 3, pp. 266–274, 2005.
[25] P. M. Aziz, H. V. Sorensen, and J. van der Spiegel, "An overview of sigma–delta converters," *IEEE Signal Process. Mag.*, vol. 13, no. 1, pp. 61–84, Jan. 1996.
[26] S.-H. Yu and J. Hu, "Stability and performance of single-bit sigma–delta modulators operated in quasi-sliding mode," *Circuits Syst. Signal Process.*, vol. 25, no. 5, pp. 571–590, 2006, (EI / SCI, IF:0.184).
[27] S. H. Yu, "Analysis and design of single-bit sigma–delta modulators using the theory of sliding modes," *IEEE Trans. Control Syst. Technol.*, vol. 14, no. 2, pp. 336–345, Mar. 2006.

Jwu-Sheng Hu (M'94) received the B.S. degree from the Department of Mechanical Engineering, National Taiwan University, Taipei, Taiwan, in 1984, and the M.S. and Ph.D. degrees from the Department of Mechanical Engineering, University of California, Berkeley, in 1988 and 1990, respectively.

He is currently a Professor with the Department of Electrical and Control Engineering, National Chiao Tung University, Hsinchu, Taiwan. His current research interests include microphone array signal processing, active noise control, intelligent mobile robots, and embedded systems and applications.

Keng-Yuan Chen (S'07) received the B.S. and M.S. degrees from the Department of Electrical and Control Engineering, National Chiao Tung University, Hsinchu, Taiwan, in 2003 and 2005, respectively, where she is currently working toward the Ph.D. degree.

Her main research interests include digital signal processing and class-D amplification.